Structure of tumor suppressor p53 and its intrinsically disordered N-terminal transactivation domain

Mark Wells*, Henning Tidow*, Trevor J. Rutherford*, Phineus Markwick†, Malene Ringkjobing Jensen†, Efstratios Mylonas‡, Dmitri I. Svergun‡§, Martin Blackledge†¶, and Alan R. Fersht*¶

*MRC Centre for Protein Engineering, Hills Road, Cambridge CB2 0QH, United Kingdom; ‡European Molecular Biology Laboratory, Hamburg Outstation, Notkestrasse 85, 22603 Hamburg, Germany; §Institute of Crystallography, Russian Academy of Sciences, Leninsky pr. 59, 117333 Moscow, Russia; and †Institut de Biologie Structurale Jean-Pierre Ebel, Unité Mixte de Recherche 5075, Centre National de la Recherche Scientifique/Commissariat à l'Energie Atomique/Université Joseph Fourier, 41 Rue Jules Horowitz, 38027 Grenoble, France

Contributed by Alan R. Fersht, February 11, 2008 (sent for review January 16, 2008)

Proteins with intrinsically disordered domains are implicated in a vast range of biological processes, especially in cell signaling and regulation. Having solved the quaternary structure of the folded domains in the tumor suppressor p53 by a multidisciplinary approach, we have now determined the average ensemble structure of the intrinsically disordered N-terminal transactivation domain (TAD) by using residual dipolar couplings (RDCs) from NMR spectroscopy and small-angle x-ray scattering (SAXS). Remarkably, not only were we able to measure RDCs of the isolated TAD, but we were also able to do so for the TAD in both the full-length tetrameric p53 protein and in its complex with a specific DNA response element. We determined the orientation of the TAD ensemble relative to the core domain, found that the TAD was stiffer in the proline-rich region (residues 64–92), which has a tendency to adopt a polyproline II (PPII) structure, and projected the TAD away from the core. We located the TAD in SAXS experiments on a complex between tetrameric p53 and four Taz2 domains that bind tightly to the TAD (residues 1–57) and acted as ''reporters.'' The p53-Taz2 complex was an extended cross-shaped structure. The quality of the SAXS data enabled us to model the disordered termini and the folded domains in the complex with DNA. The core domains enveloped the response element in the center of the molecule, with the Taz2-bound TADs projecting outward from the core.

hybrid methods | natively unfolded | protein | residual dipolar coupling | small-angle x-ray scattering

The tumor suppressor p53 is a multifunctional protein that plays vital roles in maintaining the integrity of the human genome, controlling apoptosis, cell-cycle arrest, and DNA repair (1). p53 is a homotetramer, with folded tetramerization and core domains that are linked together and flanked by intrinsically disordered (or natively unfolded) domains at the N and C termini (1, 2). As such, with 37% of its structure intrinsically disordered, p53 is typical of the structural content of the human proteome. More than 30% of eukaryotic genomes encode contiguous unfolded regions longer than 30 aa in length, and up to 80% in cancer-associated proteins (3). This new class of intrinsically disordered proteins (IDPs) is involved in a vast range of cellular processes, including molecular recognition, transcription and transposition, packaging, repair and replication, as well as signaling, cell cycle control, multiprotein complex assembly, and endocytosis. Many partly or fully disordered proteins undergo conformational transitions to folded forms only on interaction with a target ligand (4). An intrinsically disordered domain is possibly an essential structural feature that facilitates promiscuous binding to many partner proteins and is also readily accessible for posttranslational modification that modulates binding.

Solving the structures of proteins with intrinsically disordered domains now represents a major stumbling block in relating structure and biological function. Classical x-ray crystallography is difficult because such proteins usually do not crystallize, and if they did, crystal packing forces might lead to unrepresentative conformations of the disordered regions and, indeed, the whole quaternary structure. The presence of conformational flexibility requires application of methods that probe the structure in solution. To this end, we are employing a simple strategy to solve the structure of p53 (5). The first step is to solve the structures of individual core domains by using x-ray crystallography (6, 7) and NMR (8–10). The second is to solve the quaternary structure of the protein. To do this, we employ NMR spectroscopy to verify the tertiary structures of individual domains in the intact protein and identify domain–domain interactions by comparing spectra of the intact proteins with those of individual domains. Then, small-angle x-ray scattering (SAXS) is used to compute the most likely arrangement of folded domains in the full-length protein. These data may be combined, if possible, with electron microscopy on the immobilized protein. It is crucial to verify the properties of a conformationally mobile protein in solution with those of the immobilized protein (5).

Here, we proceed to the third stage of structural characterization: analyzing the ensemble of structures of the functionally important intrinsically disordered domains, beginning with the N-terminal domain of p53. This domain comprises residues 1–93, and is made up of two distinct regions; a proline-rich region (PRR, residues 64–92), attached directly to the core of the protein, and the transactivation domain (TAD) comprising the first 58 aa. The transcriptional coactivator p300 binds to p53, and a complex between tetrameric p53 and p300 has recently been proposed in which four domains of p300 wrap around the four transactivation domains of p53 (11). We have been able to use extensive measurement of residual dipolar couplings (RDCs) (12) to characterize the local structure and dynamics of the disordered domain N-terminal domain [p53(1–93)] as part of the full-length 175-kDa protein (flp53) (13–16). We combine this local conformational detail with the highly complementary definition of overall dimensions available from SAXS to provide a coherent picture of the entire protein.

Nascent Local Structure in p53(1–93)

RDC analysis showed that the isolated domain p53(1–93) was an IDP with two regions of nascent secondary structure. The TAD was previously reported to be intrinsically disordered with a tendency for helical structure in TAD1 (residues 18–25) (17),

Author contributions: M.W., H.T., T.J.R., M.B., and A.R.F. designed research; M.W., H.T., T.J.R., P.M., M.R.J., and E.M. performed research; M.B. contributed new reagents/analytic tools; M.W., E.M., D.I.S., and M.B. analyzed data; and M.W., H.T., M.B., and A.R.F. wrote the paper.

The authors declare no conflict of interest.

¶To whom correspondence may be addressed. E-mail: martin.blackledge@ibs.fr or arf25@cam.ac.uk.

This article contains supporting information online at www.pnas.org/cgi/content/full/0801353105/DCSupplemental.

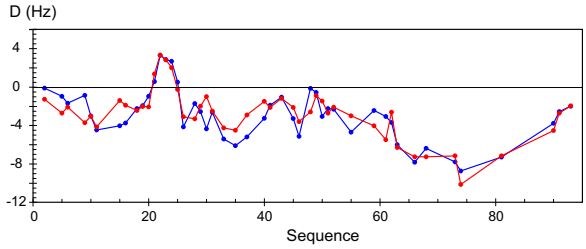

Fig. 1. NH^N RDCs from p53(1–93) in phage measured at 800 MHz compared with predicted values. NH^N RDCs from p53(1–93) (blue) were compared with predicted values (red) from amino acid-specific statistical coil predictions including the presence of a single-turn helix at residues 22–24, populated at a level of 30% and an increased level of polyproline II sampling for each amino acid in the sequence 58–91. Helical values were centered on the conformations present in the x-ray crystal structure of the α-helix formed when p53(1–93) binds to the ubiquitin ligase MDM2. All simulated values are scaled by the same prefactor to best reproduce the experimental data.

which becomes fully helical on binding to MDM2 (18). RDCs measured in intrinsically unfolded proteins have been successfully modeled by using residue-specific ϕ/ψ propensities from a coil library consisting of nonsecondary structural elements of folded proteins (19, 20). The flexible-meccano (FM) approach samples these propensities, in combination with simple volume exclusion, to generate a large number of conformers from which ensemble average properties can be predicted (21–23).

$^1D_{NHN}$ RDCs measured from p53(1–93) aligned in strained polyacrylamide gel (PAGE) and pf1 bacteriophage had similar distributions [supporting information (SI) Fig. S1], indicating that at physiological ionic strength, alignment in bacteriophage produced predominantly steric alignment of the unfolded domain. These couplings showed some similarities to values predicted by using FM (Fig. S2*A*), in reasonable agreement with the coil model over most of the transactivation domain (residues 1–57). The most significant deviation from prediction was found at residues 21–25 and over the range 58–90. Deviation in these regions was also found in other RDCs ($^2D_{C'HN}$, $^1D_{C'C\alpha}$, and $^1D_{C\alpha H\alpha}$) measured in p53 aligned in PAGE (Fig. S3*A*). Positive NH^N RDCs were observed at residues 21–25, indicating the presence of residual α-helical segments (15, 22, 24), consistent with the known propensity of residues 18–25 to form an α-helix on binding to MDM2 (18) and previous NMR studies (25). We modeled the possible conformational propensities of these amino acids by using a series of helical models, including 3_{10} and α-helical conformations, and incorporated these propensities into the FM sampling. We thus identified a 4-aa section of helical structure, populated at a level of ≈30% for residues 22–25. Using the helical conformations from the x-ray crystal structure resulted in good agreement with $^1D_{NHN}$ (Fig. 1) as well as $^2D_{C'HN}$, $^1D_{C'C\alpha}$, and $^1D_{C\alpha H\alpha}$ experimental data (Fig. S3). This observation is in agreement with $^3J_{HNH\alpha}$ couplings measured on the 73-aa N-terminal segment, which show more helical propensity in the region 21–24 than for the remainder of the MDM2 binding site (17).

High Stiffness of the PRR

An important finding is that the PRR exhibits an elevated degree of stiffness. Measured NH^N RDCs for residues 58–90 were more negative than those expected from the standard FM simulation, where average levels of polyproline II ϕ/ψ angles of (66 ± 5% and 33 ± 3%) for proline and preproline residues are present (Fig. S2 and Fig. S3). Accelerated molecular dynamics (AMD) simulations of the sequence 70–82 in the central part of the PRR predicted an increased preference for polyproline II (PPII) of (78 ± 3% and 46 ± 4% for proline and preproline, respectively) (Fig. S4). Incorporating increasing levels of PPII population into the FM ensembles for the PRR and comparing these with all experimental RDCs resulted in the identification of optimal propensities of (79 ± 2% and 50 ± 2% for proline and preproline residues, respectively), corresponding closely to those predicted from AMD. The reproduction of $^1D_{NHN}$ and $^2D_{C'HN}$, $^1D_{C'C\alpha}$, and $^1D_{C\alpha H\alpha}$ are shown in Fig. 1 and Fig. S3, respectively. Repetition of the FM calculations explicitly incorporating backbone dihedral angles extracted from the AMD simulations for amino acids 70–82 resulted in similarly well reproduced RDCs from this region (data not shown).

To overcome the spectral overlap in the PRR, we made a series of synthetic peptides comprising residues 61–93 of p53 containing ^{15}N at specific positions in the backbone. NH^N RDCs from each peptide were measured under matched alignment conditions, allowing a more detailed analysis of the conformational properties of this isolated region of the protein. The reproduction of RDCs by using FM when sampling the increased levels of PPII identified above, compared with the standard coil sampling (Fig. S5), strongly substantiated the observation that the PPII conformations were preferentially occupied in the PRR.

The polyproline II and extended β-basins of the Ramachandran plot are distinguished almost entirely by their ϕ backbone dihedral angles, with ranges of $-75 \pm 15°$ and $-120 \pm 30°$, respectively (26, 27). $^3J_{H\alpha HN}$ coupling constants were measured for the p53(61–93) peptide series. Except for V73, all of the coupling constants were in the range of 5.8–6.4 Hz, consistent with ensemble average ϕ angles within the PPII range.

Complementary sources of experiment and simulation, therefore, independently indicated that the PRR had a consistent propensity to populate elevated levels of PPII-type extended structure. This level was higher than would be expected from isolated amino acid-specific populations, suggesting the existence of some cooperative effects. The effect of this raised population of PPII conformations on the properties of the peptide chain is to stiffen the chain, as can be gauged by the increased effective persistence length, compared with simulations using the native propensities of the amino acid sequence or the TAD domain (*SI Text*, Fig. S6). Further, the PPII-type conformation might facilitate interaction of the TAD with SH3 domains, e.g., kinases.

SAXS Analysis of p53(1–93)

SAXS data were accurately reproduced by intensity curves simulated from the ensemble of p53(1–93) conformers that reproduced the RDC data (shown in the form of a semilogarithmic and a Kratky-type plot in Fig. 2), demonstrating that the overall shape of the predicted and measured ensembles was consistent with the model of the unfolded chain described above. The SAXS profile was not consistent with a collapsed structure of the transactivation domain, reported from paramagnetic relaxation enhancement experiments (Fig. S7) (28).

RDC of TAD in Full-Length p53

All experiments used a quadruple mutant flp53 that contains stabilizing mutations in the core that do not perturb the structure or impair activity (6). We were able to measure NH^N RDCs for both flp53 and its complex with a DNA target sequence, p53(1–393)–DNA. The fine structure and sign of the measured RDCs for both corresponded to those observed within p53(1–93) (Fig. 3). There were, however, striking differences in the relative size and distribution of the measured RDCs in the flp53 samples, even under conditions of similar overall alignment (as gauged by the observed ^2H quadrupolar splittings). In the presence of DNA, the TAD of flp53 had smaller couplings than those in p53(1–93), whereas the PRR had increased values. In the absence of DNA, the RDCs were very similar to those measured for p53(1–93), but RDCs from the PRR were smaller. To understand the experimental results more quantitatively, we

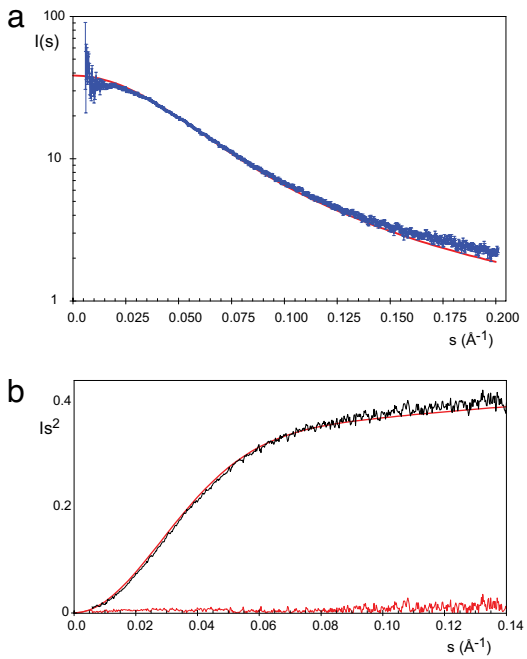

Fig. 2. Comparison of experimental and predicted SAXS data of p53(1–93). (*a*) Experimental SAXS data from p53(1–93) (blue) compared with the average simulated data using the FM ensemble calculated by using CRYSOL (red). (*b*) Kratky plots of the experimental data (black) compared with Kratky plots of the sampling by using enhanced PPII populations (red). The residuals between experiment and simulation are shown at the bottom of the plot.

explicitly modeled the conformational ensemble representing flp53–DNA.

Modeling Full-Length p53–DNA Complex

The structure of the p53(96–360) construct (comprising the core domain, linker, and tetramerization domains) in complex with DNA, determined by EM and SAXS (5) was used as the starting point of this model. An ensemble of 50,000 tetramer structures was generated, each with four independent N-terminal domain chains built into the p53 tetramer, by using an conformational sampling model identical to that used to reproduce RDCs from the isolated N-terminal domain. Similarly, the 33 aa in the C-terminal unfolded region were built onto each conformer by using randomly sampled statistical coil sampling. RDCs were predicted for each conformer on the basis of the molecular shape and size. Simulated RDCs were averaged over all 200,000 N-terminal chains in the ensemble of tetramers. A subensemble of full-length p53 conformers is represented in Fig. 4, where the proline-rich region can be seen to preferentially project the chain away from the core domain, thereby defining the volume space occupied by the flexible TAD. The resulting RDC distributions are compared with experimental values in Fig. 3*B*.

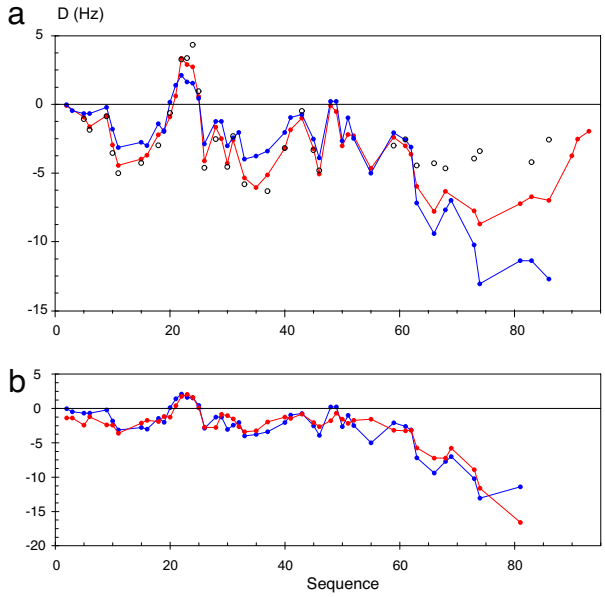

Fig. 3. RDCs from the N-terminal domain of flp53 in free and DNA-bound forms. (*a*) NH^N RDCs from residues 1–93 of p53(1–393) (open circles), p53(1–393)–DNA (blue circles), and p53(1–93) (red circles) aligned in phage at 800 MHz. (*b*) Comparison of experimental NH^N RDCs from p53(1–393)–DNA (blue circles) with predictions from model of DNA bound form (red circles).

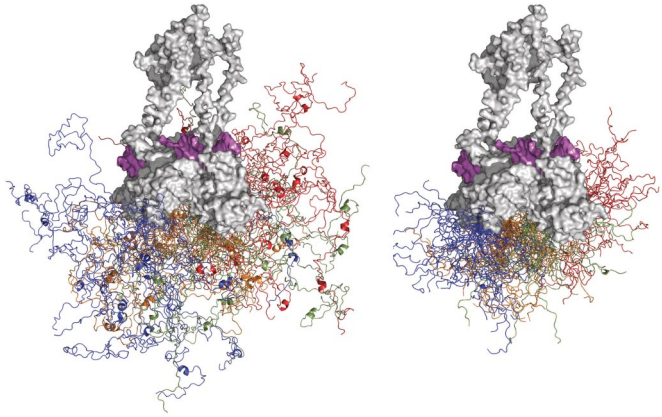

Fig. 4. Modeling the N-terminal domain in the p53–DNA complex. Shown is the N-terminal domain ensemble in our model with one representative full-length p53 molecule included for illustration. p53CTetD (gray) and DNA (magenta) are shown in space fill mode. The flexible C-terminal domain is not shown for reasons of clarity. N-terminal domains forming the four difference monomers are shown in different colors for clarity. Twenty copies are shown for each monomer. *Left* contains the entire N-terminal domain (TAD+PRR); *Right* shows only the PRR.

Although the absolute level of alignment is difficult to predict from simulation, the model closely reproduced both the decrease in the magnitude of RDC observed in the TAD and the increase in the PRR. The reproduction of the experimental data also demonstrated that, despite significant differences in measured RDCs in the isolated and DNA-bound flp53, residues 1–93 retained the same conformational preferences in p53(1–393)–DNA as they do in p53(1–93). This observation underlines the importance of considering all components of the molecular system when interpreting experimental RDCs.

The same conformational ensemble was used to predict the recently measured SAXS data from flp53–DNA (5) (Fig. S8). Beyond the initial angle region ($q < 0.04$), where experimental values are higher than prediction, reproduction of the SAXS curve was reasonable.

In the DNA-bound form, where the quaternary arrangement of folded domains is rigid and well defined, the alignment of the whole system was dominated by a single rigid body. The high degree of order experienced by the folded tetramer is efficiently propagated into the PRR, because of the relatively long persistence length, or high rigidity, of this sequence, leading to higher NH^N RDCs. In the TAD the local orientational sampling becomes less correlated to the alignment of the core domain because of a shorter persistence length and a much weaker propagated influence of the folded domain. The presence of the large body still dominates the alignment of the entire molecule

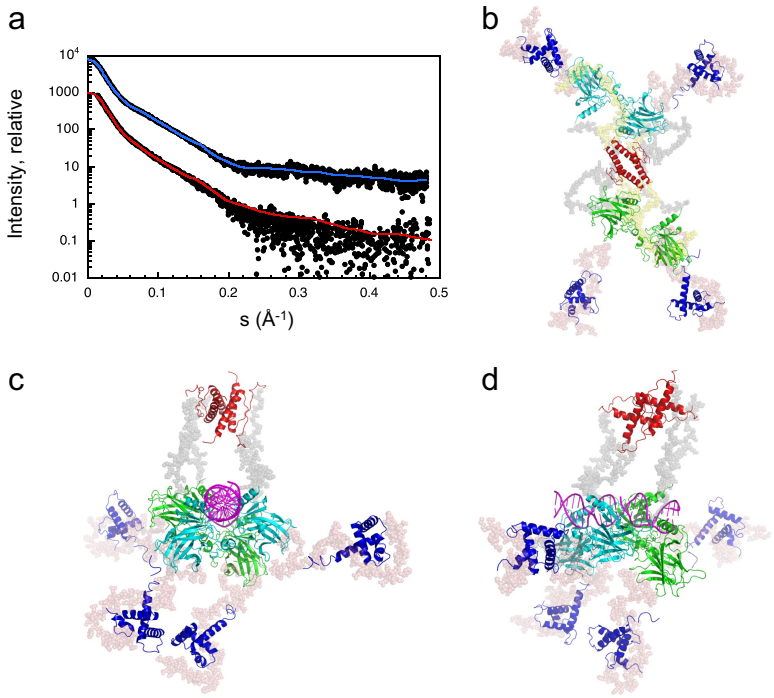

Fig. 5. SAXS models of p53–Taz2 complex and p53–Taz2–DNA complex. (*a*) SAXS analysis of p53–Taz2 complexes. Shown are the experimental intensities and fits computed from the structural models by rigid body modeling: p53+Taz2 (blue) and p53+Taz2+DNA (red). The scattering profiles are displaced along the ordinate for better visualization. (*b*) SAXS model of full-length p53–Taz2 complex in solution from rigid-body analysis and addition of missing fragments. Core domains (green and cyan), tetramerization domain (red), and Taz2 (blue) are displayed in a cartoon representation, connecting linkers (gray), N termini (salmon), and C termini (yellow) in semitransparent space fill mode. (*c* and *d*) Rigid-body model of a p53–Taz2–DNA complex from SAXS data. Core domains (green and cyan), tetramerization domain (red), Taz2 (blue), and DNA (magenta) are shown in a cartoon representation, connecting linkers (gray) and N termini (salmon) in semitransparent space fill mode. *c* and *d* represent two orthogonal views.

and therefore the same conformational sampling in the TAD leads to more efficient quenching of the RDCs.

In contrast, in the absence of a target DNA sequence, the structure of the p53 tetramer was much more dynamic than flp53–DNA, with two core-domain dimers attached to the tetramerization domain by flexible linkers. The dynamic nature of the quaternary arrangement of the component domains of isolated p53 would be expected to reduce the average alignment of the core domain of this form of the molecule. This may also account for the apparent decoupling of the effective alignment of the TAD, and the PRR experiencing more isotropic behavior than in the DNA-bound form. Modeling the N terminus in the context of flp53, which contains several rigid bodies in a highly dynamic state is beyond the scope of the present study. As discussed above, however, the RDCs from flp53 supported identical conclusions about the behavior of the N terminus in this context, and provided further evidence that the DNA free form is significantly more flexible.

Structure of flp53–Taz2 Complex from SAXS

The Taz2 domain of the transcriptional coactivator p300 binds tightly to the TAD of p53 (11). The processed SAXS patterns from flp53–Taz2 complex [scattering intensity I vs. momentum transfer $s = 4\pi(\sin\theta)/\lambda$, where 2θ is the scattering angle and λ = 1.5 Å is the wavelength] are displayed in Fig. 5*a* and the overall parameters indicate monodisperse solutions with four Taz2 bound per flp53 tetramer. To generate a structural model for the flp53–Taz2 complex, we performed rigid-body refinement by using the SAXS models for free p53 as previously described (5) and the high-resolution structure of Taz2 (PDB ID code 1F81) (29) as starting points. The final model fits the scattering pattern with discrepancy χ = 1.19 (Fig. 5*b*). Four Taz2 domains bind to the four N-terminal TADs that were shown to be extended and flexible in unbound tetrameric p53 (5). The cross-shaped scaffold consisting of a tetramerization domain in the middle with two loosely coupled core domain dimers at either end is preserved in the flp53–Taz2 complex.

Structure of an flp53–Taz2–DNA Complex from SAXS

We similarly generated a structural model for a ternary flp53–Taz2-DNA complex. Both Taz2 and a 24-residue *gadd45* response element DNA bind p53 with K_d in the low nanomolar range (11, 30, 31) and the complex was monodisperse (data not shown). The processed experimental pattern and the fit of the model are displayed in Fig. 5*a*. The structure has four core domains bound to DNA as described by Kitayner *et al.* (32) connected to the tetramerization domain by linkers. The N termini with one Taz2 molecule bound to each TAD pointed away from the core domain–DNA complex (Fig. 5*c*). These models, which are probably representative of a dynamic ensemble of conformations, agreed very well with the volume space defined by the flp53–DNA model generated from RDC data (Fig. 4).

It is notable that we could generate a model for the ternary flp53–Taz2-DNA complex that fitted the experimental data well (χ = 2.0). Previously for the flp53–DNA complex, we could only generate a model for the p53 CTetD–DNA parts of the complex and attempts to add the termini by using a static model failed (5). This indicates that the higher flexibility of the N terminus within the flp53–DNA complex may be reduced when Taz2 is bound to the N-terminal TAD.

Conclusions

The inherent flexibility of unfolded protein domains requires the development of new approaches to characterize their behavior in terms of rapidly interconverting conformational ensembles. By using RDCs, in combination with SAXS and MD simulation, we were able to identify differential flexibility in the N-terminal unfolded domain of p53. The PRR, attached to the folded core domain, exhibits enhanced stiffness relative to the TAD, projecting the TAD away from the surface of the protein, and supporting previous suggestions based on mutagenesis, that the domain plays a predominantly structural role (33). In the TAD, where chain flexibility is higher overall, we were able to identify the presence of a single helix turn, populated to ≈30%, consistent with earlier identification of a nascent helix that becomes fully helical on interaction with MDM2 (17, 18). Finally, the dynamic properties of the unfolded chain allow the measurement of RDCs from this region in the free full-length protein and in complex with DNA. In combination with previous SAXS and EM data, these data allow us to propose a residue resolution model of the full conformational sampling of flp53–DNA. The results indicated that local conformational sampling of the N-terminal domain is remarkably similar in both full-length p53 and in isolation, and substantiate previous suggestions that, although flp53–DNA is more compact and relatively rigid, the quaternary structure of the molecule is more flexible in the absence of DNA. By using a protein domain, Taz2, that binds to the TAD tightly, we could visualize the positions of the TAD-bound domain relative to the folded domains of p53.

Methods

Full details are in the *SI Text*. Proteins were expressed as in refs. 11 and 34–36. All protein samples were dialyzed into 25 mM Bis-Tris·HCl, pH 6.8, 150 mM NaCl, pH 6.8, containing 10% ^2H_2O for NMR studies. Gels were used for RDC measurements as in ref. 37, and spectra were recorded at 20°C by using standard Bruker pulse sequences and methods described in refs. 38–42. The SAXS data were collected at the X33 beamline at EMBL/DESY, Hamburg (43), following standard procedures. The p53(1–93) ranged from 2 to 8.6 mg/ml in 25 mM phosphate, pH 7.2, 150 mM NaCl, 5 mM DTT, 5% (vol/vol) glycerol. Data were processed by using PRIMUS (44). Further analysis and modeling were performed by using the ATSAS package (45) with programs CRYSOL (46), SASREF, and BUNCH (47). Side chains were added to the conformers generated by the FM method in the unfolded domains by using the SCCOMP program (48). Accelerated molecular dynamic (AMD) simulations (49, 50) used an in-house modified version of the sander module in AMBER8 (51).

ACKNOWLEDGMENTS. We thank C. Blair (MRC Centre for Protein Engineering) for TEV protease, Dr. D. Teufel (MRC Centre for Protein Engineering) for Taz2 protein, and Drs. S. Freund and T. Religa for assistance with NMR spectroscopy. This work was supported by European Community–Research Infrastructure Action under the FP6 (RII3/CT/2004/5060008) for access to EMBL/DESY, Hamburg, and by French research ministry Grant ANR NT05-4_42781. H.T. was supported by a fellowship from the Boehringer Ingelheim Fonds and by a Trinity College Junior Research Fellowship.

1. Joerger AC, Fersht AR (2007) Structure-function-rescue: The diverse nature of common p53 cancer mutants. *Oncogene* 26:2226–2242.
2. Romer L, Klein C, Dehner A, Kessler H, Buchner J (2006) p53—A natural cancer killer: Structural insights and therapeutic concepts. *Angew Chem Int Ed* 45:6440–6460.
3. Iakoucheva LM, Brown CJ, Lawson JD, Obradovic Z, Dunker AK (2002) Intrinsic disorder in cell-signaling and cancer-associated proteins. *J Mol Biol* 323:573–584.
4. Fink AL (2005) Natively unfolded proteins. *Curr Opin Struct Biol* 15:35–41.
5. Tidow H, *et al.* (2007) Quaternary structures of tumor suppressor p53 and a specific p53 DNA complex. *Proc Natl Acad Sci USA* 104:12324–12329.
6. Joerger AC, Allen MD, Fersht AR (2004) Crystal structure of a superstable mutant of human p53 core domain. Insights into the mechanism of rescuing oncogenic mutations. *J Biol Chem* 279:1291–1296.
7. Cho Y, Gorina S, Jeffrey PD, Pavletich NP (1994) Crystal structure of a p53 tumor suppressor-DNA complex: Understanding tumorigenic mutations. *Science* 265:346–355.
8. Canadillas JM, *et al.* (2006) Solution structure of p53 core domain: Structural basis for its instability. *Proc Natl Acad Sci USA* 103:2109–2114.
9. Clore GM, *et al.* (1995) Refined solution structure of the oligomerization domain of the tumour suppressor p53. *Nat Struct Biol* 2:321–333.
10. Lee W, *et al.* (1994) Solution structure of the tetrameric minimum transforming domain of p53. *Nat Struct Biol* 1:877–890.
11. Teufel DP, Freund SM, Bycroft M, Fersht AR (2007) Four domains of p300 each bind tightly to a sequence spanning both transactivation subdomains of p53. *Proc Natl Acad Sci USA* 104:7009–7014.
12. Tjandra N, Bax A (1997) Direct measurement of distances and angles in biomolecules by NMR in a dilute liquid crystalline medium. *Science* 278:1111–1114.
13. Shortle D, Ackerman MS (2001) Persistence of native-like topology in a denatured protein in 8 M urea. *Science* 293:487–489.
14. Louhivuori M, *et al.* (2003) On the origin of residual dipolar couplings from denatured proteins. *J Am Chem Soc* 125:15647–15650.
15. Mohana-Borges R, Goto NK, Kroon GJ, Dyson HJ, Wright PE (2004) Structural characterization of unfolded states of apomyoglobin using residual dipolar couplings. *J Mol Biol* 340:1131–1142.
16. Meier S, Grzesiek S, Blackledge M (2007) Mapping the conformational landscape of urea-denatured ubiquitin using residual dipolar couplings. *J Am Chem Soc* 129:9799–9807.
17. Lee H, *et al.* (2000) Local structural elements in the mostly unstructured transcriptional activation domain of human p53. *J Biol Chem* 275:29426–29432.
18. Kussie PH, *et al.* (1996) Structure of the MDM2 oncoprotein bound to the p53 tumor suppressor transactivation domain. *Science* 274:948–953.
19. Bernado P, *et al.* (2005) A structural model for unfolded proteins from residual dipolar couplings and small-angle x-ray scattering. *Proc Natl Acad Sci USA* 102:17002–17007.
20. Jha AK, Colubri A, Freed KF, Sosnick TR (2005) Statistical coil model of the unfolded state: Resolving the reconciliation problem. *Proc Natl Acad Sci USA* 102:13099–13104.
21. Bernado P, Bertoncini CW, Griesinger C, Zweckstetter M, Blackledge M (2005) Defining long-range order and local disorder in native alpha-synuclein using residual dipolar couplings. *J Am Chem Soc* 127:17968–17969.
22. Mukrasch MD, *et al.* (2007) Highly populated turn conformations in natively unfolded Tau protein identified from residual dipolar couplings and molecular simulation. *J Am Chem Soc* 129:5235–5243.
23. Meier S, Guthe S, Kiefhaber T, Grzesiek S (2004) Foldon, the natural trimerization domain of T4 fibritin, dissociates into a monomeric A-state form containing a stable beta-hairpin: Atomic details of trimer dissociation and local beta-hairpin stability from residual dipolar couplings. *J Mol Biol* 344:1051–1069.
24. Fieber W, Kristjansdottir S, Poulsen FM (2004) Short-range, long-range and transition state interactions in the denatured state of ACBP from residual dipolar couplings. *J Mol Biol* 339:1191–1199.
25. Mohan A, *et al.* (2006) Analysis of molecular recognition features (MoRFs). *J Mol Biol* 362:1043–1059.
26. Swindells MB, MacArthur MW, Thornton JM (1995) Intrinsic phi, psi propensities of amino acids, derived from the coil regions of known structures. *Nat Struct Biol* 2:596–603.
27. Shi ZS, Chen K, Liu ZG, Kallenbach NR (2006) Conformation of the backbone in unfolded proteins. *Chem Rev* 106:1877–1897.
28. Vise P, Baral B, Stancik A, Lowry DF, Daughdrill GW (2007) Identifying long-range structure in the intrinsically unstructured transactivation domain of p53. *Proteins* 67:526–530.
29. De Guzman RN, Liu HY, Martinez-Yamout M, Dyson HJ, Wright PE (2000) Solution structure of the TAZ2 (CH3) domain of the transcriptional adaptor protein CBP. *J Mol Biol* 303:243–253.
30. Ang HC, Joerger AC, Mayer S, Fersht AR (2006) Effects of common cancer mutations on stability and DNA binding of full-length p53 compared with isolated core domains. *J Biol Chem* 281:21934–21941.
31. Weinberg RL, Veprintsev DB, Fersht AR (2004) Cooperative binding of tetrameric p53 to DNA. *J Mol Biol* 341:1145–1159.
32. Kitayner M, *et al.* (2006) Structural basis of DNA recognition by p53 tetramers. *Mol Cell* 22:741–753.
33. Toledo F, *et al.* (2007) Mouse mutants reveal that putative protein interaction sites in the p53 proline-rich domain are dispensable for tumor suppression. *Mol Cell Biol* 27:1425–1432.
34. Yu GW, *et al.* (2006) The central region of HDM2 provides a second binding site for p53. *Proc Natl Acad Sci USA* 103:1227–1232.
35. Nikolova PV, Henckel J, Lane DP, Fersht AR (1998) Semirational design of active tumor suppressor p53 DNA binding domain with enhanced stability. *Proc Natl Acad Sci USA* 95:14675–14680.
36. Veprintsev DB, *et al.* (2006) Core domain interactions in full-length p53 in solution. *Proc Natl Acad Sci USA* 103:2115–2119.
37. Chou JJ, Gaemers S, Howder B, Louis JM, Bax A (2001) A simple apparatus for generating stretched polyacrylamide gels, yielding uniform alignment of proteins and detergent micelles. *J Biomol NMR* 21:377–382.
38. Permi P, Rosevear PR, Annila A (2000) A set of HNCO-based experiments for measurement of residual dipolar couplings in N-15, C-13 (H-2)-labeled proteins. *J Biomol NMR* 17:43–54.
39. Yang DW, Tolman JR, Goto NK, Kay LE (1998) An HNCO-based pulse scheme for the measurement of C-13(alpha)-H-1(alpha) one-bond dipolar couplings in N-15, C-13 labeled proteins. *J Biomol NMR* 12:325–332.
40. Permi P, Heikkinen S, Kilpelainen I, Annila A (1999) Measurement of (1)J(NC′) and (2)J(HNC′) couplings from spin-state-selective two-dimensional correlation spectrum. *J Magn Reson* 140:32–40.

41. Vuister GW, Bax A (1993) Quantitative J correlation—A new approach for measuring homonuclear 3-bond J(H(N)H(alpha) coupling-constants in N-15-enriched proteins. *J Am Chem Soc* 115:7772–7777.
42. Delaglio F, *et al.* (1995) NMRPipe: A multidimensional spectral processing system based on UNIX pipes. *J Biomol NMR* 6:277–293.
43. Roessle MW, *et al.* (2007) Upgrade of the small-angle X-ray scattering beamline X33 at the European Molecular Biology Laboratory, Hamburg. *J Appl Crystallogr* 40:S190–S194.
44. Konarev PV, Volkov VV, Sokolova AV, Koch MHJ, Svergun DI (2003) Primus: A Windows PC-based system for small-angle x-ray scattering data analysis. *J Appl Crystallogr* 36:1277–1282.
45. Konarev PV, Petoukhov MV, Volkov VV, Svergun DI (2006) ATSAS 2.1, a program package for small-angle scattering data analysis. *J Appl Crystallogr* 39:277–286.
46. Svergun DI, Barberato C, Koch MHJ (1995) CRYSOL—A program to evaluate x-ray solution scattering of biological macromolecules from atomic coordinates. *J Appl Crystallogr* 28:768–773.
47. Petoukhov MV, Svergun DI (2005) Global rigid body modeling of macromolecular complexes against small-angle scattering data. *Biophys J* 89:1237–1250.
48. Eyal E, Najmanovich R, McConkey BJ, Edelman M, Sobolev V (2004) Importance of solvent accessibility and contact surfaces in modeling side-chain conformations in proteins. *J Comput Chem* 25:712–724.
49. Hamelberg D, McCammon JA (2005) Fast peptidyl cis-trans isomerization within the flexible Gly-rich flaps of HIV-1 protease. *J Am Chem Soc* 127:13778–13779.
50. Markwick PRL, Bouvignies G, Blackledge M (2007) Exploring multiple timescale motions in protein GB3 using accelerated molecular dynamics and NMR spectroscopy. *J Am Chem Soc* 129:4724–4730.
51. Case DA, *et al.* (2004) AMBER 8 (Univ of California, San Francisco).